

Heterogeneous Catalysis | Hot Paper |

Visible-Light-Mediated Oxidative Amidation of Aldehydes by Using Magnetic CdS Quantum Dots as a Photocatalyst

Ling Xu, Shuai-Zheng Zhang, Wei Li, and Zhan-Hui Zhang*^[a]

Dedicated to the 100th anniversary of chemistry at Nankai University

Abstract: A magnetic CdS quantum dot (Fe₃O₄/polydopamine (PDA)/CdS) was synthesized through a facile and convenient method from inexpensive starting materials. Characterization of the prepared catalyst was performed by means of FTIR spectroscopy, XRD, SEM, TEM, energy-dispersive X-ray spectroscopy, and vibrating-sample magnetometer tech-

niques. Fe₃O₄/PDA/CdS was found to be a highly active photocatalyst for the amidation of aromatic aldehydes by using air as a clean oxidant under mild conditions. The photocatalyst can be recovered by magnetic separation and successfully reused for five cycles without considerable loss of its catalytic activity.

Introduction

The continuously growing demand for the development of green and valuable transformations in organic synthesis has inspired chemists to address environmental and energy issues through an operative and scalable technology.^[1] In this context, visible-light-mediated photoredox catalysis has become a versatile and powerful strategy for reducing thermochemical or electrochemical activation energy by using safe, abundant, clean, and renewable light sources.^[2–5] However, the main contributions come from homogeneous photoredox catalysts, such as transition-metal complexes based on ruthenium or iridium, as well as various organic dyes.^[6–8] Photoredox catalysis with heterogeneous photocatalysts has the inherent advantages of easy catalyst separation and recycling and is of great interest from industrial and academic points of view.^[9–13]

The synthesis of amides is of great significance in organic synthesis, because an amide is a key functional group in materials, natural products, and medicines.^[14] Recent estimates from the U.S. patent literature suggest that amidation reactions represent approximately 15% of all transformations.^[15] To date, numerous methods for constructing amide bonds have been reported.^[16] The most well-established routes for the formation of amides involve the reaction of amines with activated carboxylic acids or their corresponding derivatives,^[17] the Schmidt reaction,^[18] the Beckmann rearrangement reaction,^[19] and

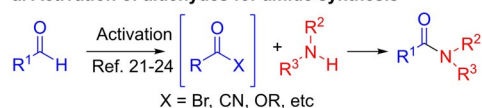
modified Staudinger reaction.^[20] From the perspective of green chemistry, these processes generate a large amount of byproducts and chemical waste, so they need to be improved or replaced. Thus, much effort is being devoted to making the formation of amide bonds more “green.” Among reported amidation reactions, the direct cross-dehydrogenative coupling (CDC) of aldehydes with amines is one of the most economical methods to prepare amides, because the starting materials are readily available and only hydrogen is produced as a byproduct.

Various methods have been reported to form amide bonds with aldehydes and amines as starting materials (Scheme 1). Aldehydes are activated by forming acyl bromides,^[21] acyl cyanides,^[22] nitriles,^[23] or active esters^[24] as intermediates and are then coupled with amines (Scheme 1 a). Amines can also be converted into *N*-chloramine^[25] or anionic amido complexes^[26] as reactive intermediates to react with aldehydes (Scheme 1 b). In addition, catalytic methods with copper,^[27] copper/silver,^[28] iron,^[29] transition metals (Pd, Rh, and Ru),^[30] and lanthanide^[31] have been reported (Scheme 1 c). However, some of these strategies have inherent shortcomings, such as the employment of expensive transition-metal catalysts, elevated temperature, or superfluous use of strong oxidants. In recent photochemical studies, visible-light photoredox catalysis has provided optional approaches for the oxidative amidation of aldehydes by using a phenazinium salt,^[32] rose Bengal,^[33] boron-dipyrromethene (BODIPY),^[34] silyl-substituted quinolinium compounds,^[35] hemicyanine derivatives (CAT),^[36] Ag/graphitic carbon nitride (g-C₃N₄),^[37] or anthraquinone (AQN)-based organophotocatalysts^[38] (Scheme 1 d). Nonetheless, most existing methods involve the use of expensive catalysts and require additives, and the separation of homogeneous photocatalysts is still problematic. All of the deficiencies mentioned above prompted us to continuously explore a less costly, greener, heterogeneous, and simpler catalyst system under base-/addi-

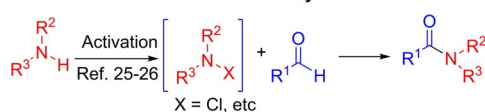
[a] L. Xu, S.-Z. Zhang, W. Li, Prof. Z.-H. Zhang
Hebei Key Laboratory of Organic Functional Molecules
National Demonstration Center for Experimental Chemistry Education
College of Chemistry and Material Science, Hebei Normal University
Shijiazhuang 050024 (P.R. China)
E-mail: zhanhui@mail.nankai.edu.cn

Supporting information and the ORCID identification numbers for the authors of this article can be found under:
<https://doi.org/10.1002/chem.202005138>

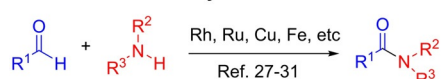
a. Activation of aldehydes for amide synthesis



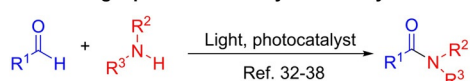
b. Activation of amines for amide synthesis



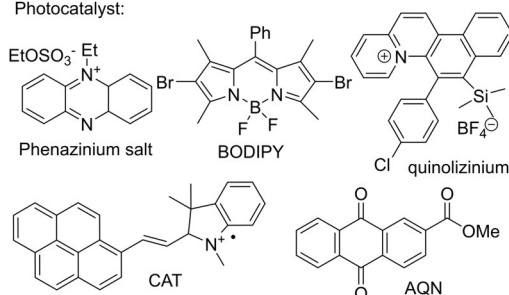
c. Transition-metal-catalyzed oxidative amidation



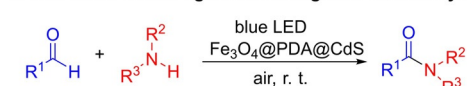
d. Visible light photoredox catalytic amide synthesis



Photocatalyst:



e. This work: Visible-light-driven magnetic CdS-catalyzed oxidative amidation



Scheme 1. Approaches for the amidation of aldehydes. LED = light-emitting diode, PDA = polydopamine.

tive-free conditions in air for industrial applications that can meet some principles of green chemistry.

Heterogeneous photocatalysis with semiconductor materials (e.g., TiO₂, CdS, ZnO, WO₃, Bi₂WO₆, and ZnWO₄) has achieved many applications due to the attractive properties of these materials.^[39–43] Among the available photoactive semiconductor materials, cadmium sulfide (CdS) has attracted widespread attention because of its narrower visible-light-response band gap (approximately 2.4 eV) and more suitable band-edge position.^[44] CdS and CdS-based composite materials have been used as photocatalysts for various critical fields, including water splitting,^[45] CO₂ reduction,^[46] nitrogen fixation,^[47] environmental pollutant treatment,^[48] and organic synthesis.^[49–56] However, the application of single-phase CdS in photocatalysis is still restricted because the recombination of photogenerated carriers occurs quickly. In addition, single-phase CdS is not photostable, and photocorrosion may occur through the oxidation process of photogenerated holes under irradiation. Another important concern of CdS photocatalysis is the leaching of Cd²⁺ ions, leading to the formation of dangerous metal ions in solution.^[57] To overcome these CdS defects, some significant achievements have been fulfilled by controlling the synthesis of CdS by increasing the surface area and tuning the crystal sizes and structures. For example, Xiang et al. reported the

preparation of 2D ultrathin CdS nanosheets by a simple one-step, solid-phase, synthetic method.^[58] This type of ultrathin nanosheet structure can prevent surface sulfide ions from being oxidized, thereby effectively inhibiting photocorrosion. In addition, coupling CdS with other semiconductors, such as Ti₃C₂T_x,^[42a] Ni₂S,^[59] W₂S,^[60] ZnS,^[61] Ag₂S,^[62] and WO₃,^[63] is an effective method to suppress the recombination of photoinduced charge pairs.

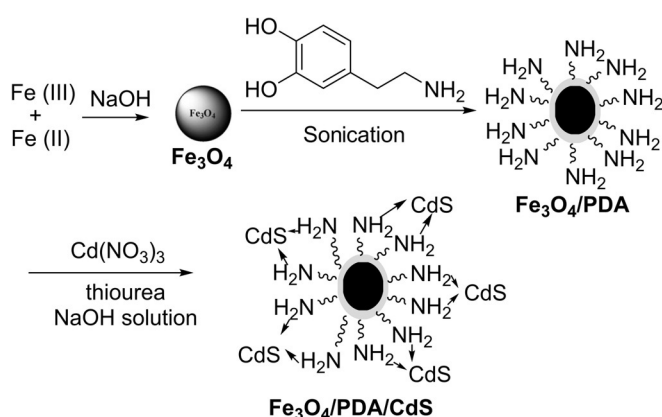
Recently, magnetite nanoparticles (MNPs) have attracted remarkable attention as a powerful catalyst support due to their unique characteristics, including chemical and heat resistance, low toxicity, simple and cheap preparation, large surface areas, and simple isolation by using external magnets. Importantly, magnetic separation is considered to be a green process that can avoid the use of filtration or centrifugation steps during the separation process.^[64] Additionally, these magnetic materials can also control the size, stabilize, and enhance the visible-light activity of CdS.^[65] More recently, some magnetic supported CdS photocatalysts have been developed. For example, Samadi-Maybodi and co-workers have synthesized Fe₃O₄/CdS nanohybrids that displayed superior photocatalytic activity toward the degradation of xlenol orange.^[66] The CdS/C@Fe₃O₄ nanoreactor has been synthesized through the surface-imprinting technique and applied as a photocatalyst in the photodegradation of ciprofloxacin.^[67] Shi and co-workers have synthesized yolk-shell-structured Fe₃O₄@void@CdS nanoparticles (NPs) that exhibited excellent photo-Fenton activity toward the degradation of methylene blue.^[68] Moreover, some novel magnetic intercalation photocatalysts, such as Fe₃O₄@SiO₂@CdS,^[69] Fe₃O₄@SiO₂@ZnO/CdS,^[70] and 2D/2D CdS/α-Fe₂O₃,^[71] have been reported.

The PDA coating is one of the simplest and most versatile approaches for the functionalization of material surfaces. PDA has the ability to absorb light over a broadband spectrum from ultraviolet to visible light.^[72] Under visible-light radiation, its photoconductivity can be greatly enhanced, implying an increase in photogenerated free electrons and electron holes. The light-energy conversion of PDA can significantly improve the catalytic activity of semiconductors and make PDA a potential light-harvesting material for photocatalysis.^[73] Mao and co-workers reported that the photocatalytic activity of TiO₂ could be significantly improved with the existence of PDA.^[74] Feng et al. prepared PDA-coated silver core-shell nanostructures for enhanced photocatalysis.^[75] Palladium NPs stabilized on PDA-coated magnetic nanocomposites have been synthesized as reusable heterogeneous catalysts.^[76] To the best of our knowledge, the application of magnetic CdS quantum dots in amide synthesis has not been reported. Based on these reasons, and as part of our ongoing research interest in the development of environmentally friendly synthetic methodologies,^[77,78] herein, we used Fe₃O₄ NPs as the core and synthesized Fe₃O₄/PDA/CdS nanocomposites, which exhibited high photocatalytic activity for the aerobic oxidative amidation of aromatic aldehydes (Scheme 1 e).

Results and Discussion

Synthesis and characterization of Fe₃O₄/PDA/CdS

The Fe₃O₄/PDA/CdS hybrid structure was fabricated through a layer-by-layer process, as outlined in Scheme 2. First, Fe₃O₄ NPs were prepared by a chemical coprecipitation technique using FeCl₃·6H₂O and FeCl₂·4H₂O as precursors. The in situ synthesized PDA molecules bind with Fe₃O₄ NPs through strong covalent bonds by using the vicinal dihydroxy group of dopamine. The obtained PDA-coated Fe₃O₄ NPs were then treated with Cd(NO₃)₂·4H₂O and thiourea to afford aminated Fe₃O₄/PDA/CdS. The free amino groups of PDA were exploited as a robust anchor and capping agent to stabilize CdS. As coordination atoms, the nitrogen atoms contained in PDA play a key role in chelating Cd^{II}.



Scheme 2. Synthesis of Fe₃O₄/PDA/CdS.

The crystal phase structure and crystallinity of the Fe₃O₄/PDA/CdS composite catalyst have a great influence on its photocatalytic activity. XRD can be used to characterize the crystal phase structure and crystallinity of the photocatalyst. Figure 1 shows a comparison of the XRD results of pure CdS nano-sheets, pure Fe₃O₄ NPs, and Fe₃O₄/PDA/CdS. The main diffraction peak positions of the obtained Fe₃O₄/PDA/CdS catalyst

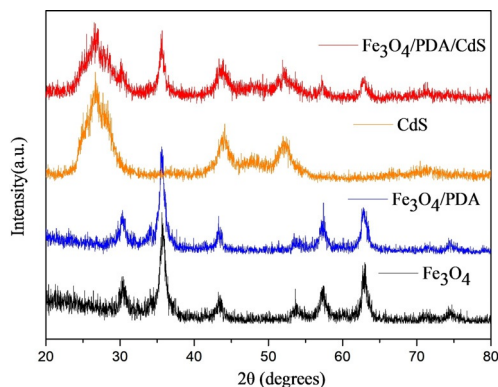


Figure 1. Powder XRD patterns of Fe₃O₄, Fe₃O₄/PDA, CdS, and Fe₃O₄/PDA/CdS composites.

appear at 26.5, 43.9, and 51.9°, which correspond to the (111), (220), and (311) crystal faces of CdS, respectively.^[48] The additional diffraction peaks at 30.1, 35.5, 43.5, 57.0, and 62.6° of the composite samples correspond to (220), (311), (400), (511), and (440) reflections of Fe₃O₄, respectively.^[64e] Furthermore, there are no other unexpected peaks, other than Fe₃O₄ and CdS, in the patterns.

SEM and TEM analyses were performed to directly analyze the microscopic structural information of the catalyst. The SEM and TEM images of MNP-supported CdS are shown in Figures 2 and 3. The TEM image of the catalyst shows that magnetic particles are highly aggregated and CdS is distributed evenly on the PDA-modified surface of the Fe₃O₄ NPs. The average size of these particles is about 60 nm. The SEM image of the catalyst confirms that these NPs are uneven-sized particles and most of the particles have a quasi-spherical shape. Meanwhile, SEM elemental mapping indicated the uniform deposition of Cd, S, Fe, O, and N elements over the entire Fe₃O₄/PDA/CdS (Figure S1 in the Supporting Information). It was revealed that CdS had been successfully immobilized on the surface of Fe₃O₄. These results further confirm the high purity of the produced Fe₃O₄/PDA/CdS structure. The amount of Cd metal in the immobilized catalyst was found to be 36.64% based on inductively coupled plasma atomic emission spectroscopy (ICP-AES) analysis.

Figure 4 shows the FTIR spectra of Fe₃O₄, Fe₃O₄/PDA, CdS, and Fe₃O₄/PDA/CdS composites. The bands at 1620, 1384, and 1106 cm⁻¹ are the characteristic absorptions of CdS. The presence of Fe–O bonds in the magnetic particles is confirmed by the characteristic band appearing at 570 cm⁻¹. The intense and

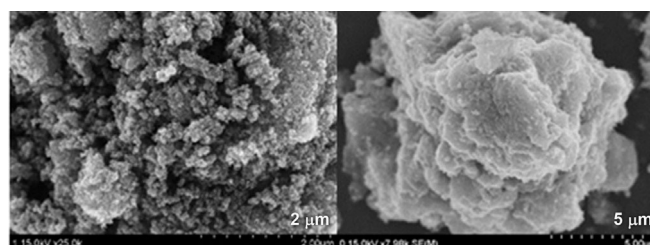


Figure 2. SEM images of Fe₃O₄ (left) and Fe₃O₄/PDA/CdS (right).

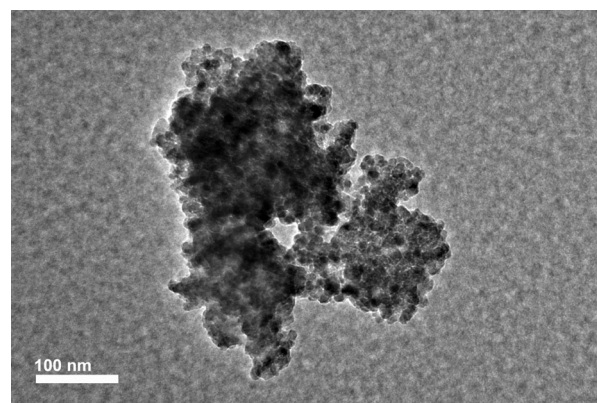


Figure 3. TEM image of Fe₃O₄/PDA/CdS.

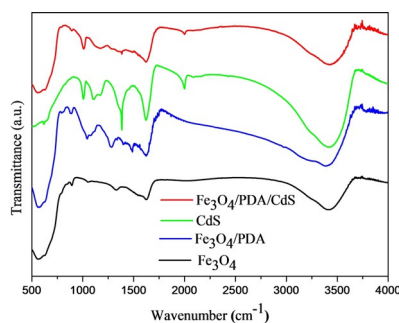


Figure 4. IR spectra of Fe_3O_4 , $\text{Fe}_3\text{O}_4/\text{PDA}$, CdS , and $\text{Fe}_3\text{O}_4/\text{PDA}/\text{CdS}$ composites.

broad bands near 3420 cm^{-1} in the three spectra are characteristic absorption bands of the vibration of $-\text{OH}$ bands, which overlap with the $-\text{NH}_2$ stretching vibration.

We further investigated the surface area, which generally has a great influence on the catalytic activity of photocatalysts. Figure 5 exhibits the nitrogen adsorption–desorption isotherms of $\text{Fe}_3\text{O}_4/\text{PDA}/\text{CdS}$. The specific surface area of $\text{Fe}_3\text{O}_4/\text{PDA}/\text{CdS}$ obtained from the N_2 adsorption isotherms was $92.8\text{ m}^2\text{ g}^{-1}$. The pore size distribution calculated by using the nonlocal density functional theory (NLDFT) method resulted in a pore diameter of 5.9 nm.

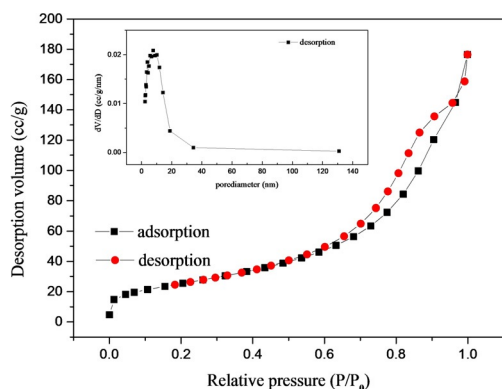


Figure 5. Nitrogen adsorption–desorption isotherms of $\text{Fe}_3\text{O}_4/\text{PDA}/\text{CdS}$.

The magnetic properties of samples of Fe_3O_4 , $\text{Fe}_3\text{O}_4/\text{PDA}$, and $\text{Fe}_3\text{O}_4/\text{PDA}/\text{CdS}$ were evaluated by means of vibrating-sample magnetometry (VSM) at room temperature. The VSM magnetization curves of magnetic NPs, before and after immobilization, exhibit superparamagnetic behavior (Figure 6). The magnetic saturation (M_{sat}) value is 59.14 emu g^{-1} for Fe_3O_4 , whereas the M_{sat} values of $\text{Fe}_3\text{O}_4/\text{PDA}$ and $\text{Fe}_3\text{O}_4/\text{PDA}/\text{CdS}$ decrease to 53.12 and 24.96 emu g^{-1} , respectively. The significantly reduced M_{sat} is probably due to the existence of a large amount of nonmagnetic material on the surface of the Fe_3O_4 particles. Even with this reduction in saturation magnetization, the prepared catalyst still retains a sufficient M_{sat} value and can be effectively separated from the reaction system through an external magnetic field.

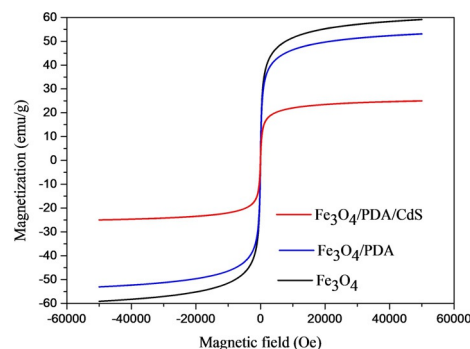



Figure 6. Magnetization curves of Fe_3O_4 , $\text{Fe}_3\text{O}_4/\text{PDA}$, and $\text{Fe}_3\text{O}_4/\text{PDA}/\text{CdS}$.

Photocatalyst activity tests

After the detailed characterization of $\text{Fe}_3\text{O}_4/\text{PDA}/\text{CdS}$, its activity as a photocatalyst in the aerobic oxidative amidation of aldehydes was studied under visible-light irradiation at room temperature. We began our investigation by using 4-nitrobenzaldehyde and pyrrolidine as model substrates. First, the effect of various solvents on the product yield was examined at room temperature (Table 1, entries 1–13). If water, acetone, γ -valerolactone, and PEG 600 were used as solvents, the desired product could not be obtained (Table 1, entries 1–4). If the reaction was conducted in ethanol, dichloromethane, *n*-hexane, and toluene, the product was isolated in low yield (Table 1, entries 5–8). The desired product was obtained in modest yields in DMF, THF, 1,4-dioxane, cyclopentyl methyl ether, and 2-MeTHF (Table 1, entries 9–13). Furthermore, we found that the reaction proceeded under solvent-free conditions to give the product in 62% yield (Table 1, entry 14). Delightfully, the reaction could work well in DMSO and CH_3CN ; the best performance was obtained in CH_3CN , giving (4-nitrophenyl)(pyrrolidin-1-yl)methanone (**3 m**) in 93% yield (Table 1, entry 16). Screening of different light sources showed that blue light slightly increased the yield. The apparent quantum efficiency (AQE) was 0.54% at 450 nm (see the Supporting Information).^[40c] Furthermore, increasing or decreasing the loading amounts of catalyst did not improve the yield (Table 1, entries 20 and 21). The photoactivity of bare CdS quantum dots was also tested, and it was found that there was a slight decrease in the yield of **3 m** (Table 1, entry 22). This indicates that the introduction of PDA significantly enhanced the light absorption and conversion of the CdS-catalyzed oxidative amidation. Finally, control experiments revealed that only traces of the product were formed in the absence of photocatalyst or without visible-light irradiation (Table 1, entries 23 and 24), thus indicating that both the catalyst and light were essential for effective conversion into **3 m**.

Amidation of aromatic aldehydes

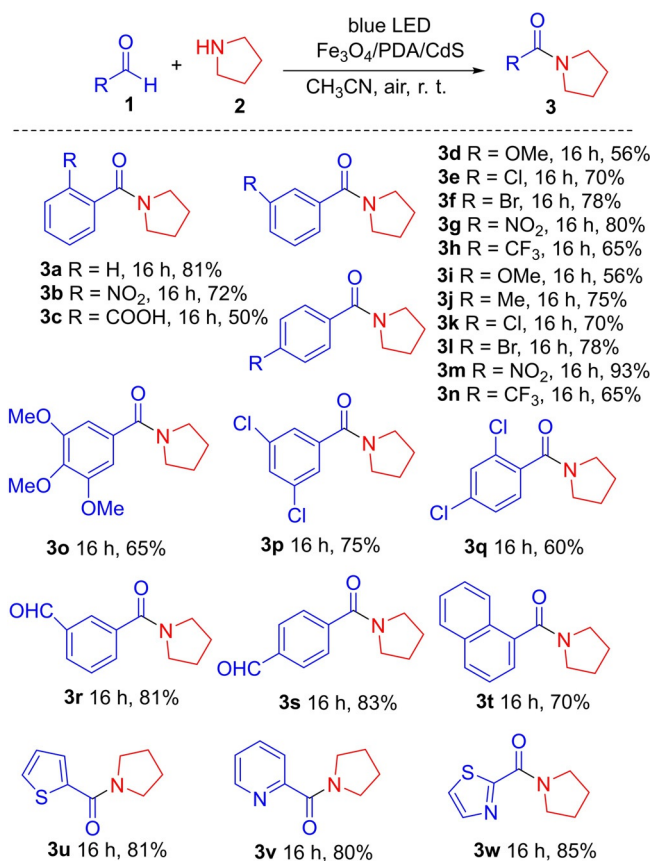
Having established the optimized conditions, we investigated the scope and generality of such transformations with various aromatic aldehydes and pyrrolidine. As highlighted in Scheme 3, representative electron-donating or -withdrawing

Table 1. Optimization of the reaction condition for reaction of 4-nitrobenzaldehyde and pyrrolidine under light irradiation.^[a]


Entry	Light source	Solvent	t [h]	Yield ^[b] [%]
1	blue LED	H ₂ O	30	trace
2	blue LED	acetone	30	trace
3	blue LED	γ -valerolactone	30	trace
4	blue LED	PEG 600 ^[c]	30	trace
5	blue LED	EtOH	16	20
6	blue LED	CH ₂ Cl ₂	16	21
7	blue LED	<i>n</i> -hexane	16	22
8	blue LED	toluene	16	23
9	blue LED	DMF	16	50
10	blue LED	THF	16	51
11	blue LED	1,4-dioxane	16	53
12	blue LED	cyclopentyl methyl ether	16	54
13	blue LED	2-Me-THF	16	60
14	blue LED	none	16	62
15	blue LED	DMSO	16	90
16	blue LED	CH ₃ CN	16	93
17	white LED	CH ₃ CN	16	75
18	ultraviolet light	CH ₃ CN	16	76
19	green LED	CH ₃ CN	16	90
20 ^[d]	blue LED	CH ₃ CN	16	80
21 ^[e]	blue LED	CH ₃ CN	16	93
22 ^[f]	blue LED	CH ₃ CN	16	88
23	dark	CH ₃ CN	36	trace
24 ^[g]	blue LED	CH ₃ CN	24	trace

[a] Reaction conditions: 4-nitrobenzaldehyde (1.0 mmol), pyrrolidine (1.0 mmol), and catalyst (20 mg, 6.4 mol% Cd) in the solvent (2.0 mL) at room temperature, in air, 18 W LEDs. [b] Yields of products isolated. [c] PEG = polyethylene glycol. [d] 10 mg catalyst was used. [e] 30 mg catalyst was used. [f] Pure CdS (9.2 mg, 6.4 mol%) was used. [g] In the absence of photocatalyst.

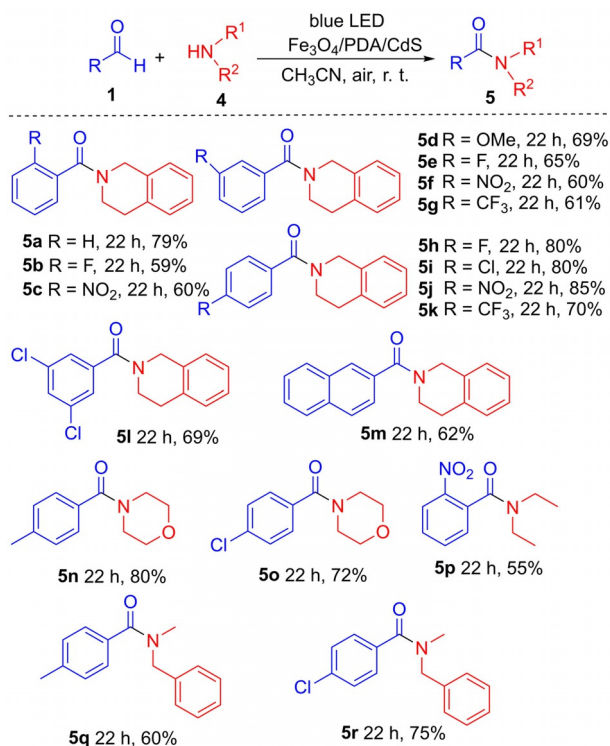
groups on the phenyl ring of benzaldehyde substrates worked well under the reaction conditions to deliver the desired products in moderate to excellent yields. The electronic effect of the aldehyde has a clear influence on the transformation. In general, high yields were observed for benzaldehydes with electron-deficient groups on the phenyl ring, whereas electron-rich aryl groups significantly reduced the yields. The influence of substituents on benzaldehyde is consistent with that reported in the literature.^[32–38] Both chloro and bromo substituents were well tolerated under the developed reaction conditions, providing an easy means for further synthetic elaboration. In particular, isophthalaldehyde and terephthalaldehyde, with two aldehyde groups, reacted with one equivalent of pyrrolidine to afford the monoamidation products **3r** and **3s** in 81 and 83% yield, respectively. It is worth noting that this protocol was also efficient for polycyclic and heterocyclic aromatic aldehydes, and the corresponding amides **3t–3w** were obtained in moderate to good yields. Unfortunately, in the case of aliphatic aldehydes as substrates, the reactions failed to afford the desired products.


Scheme 3. Substrate scope of aryl aldehydes. Standard reaction conditions. Isolated yield.

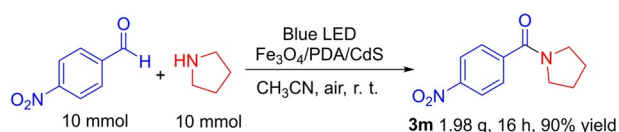
Subsequently, the scope of the reaction was explored with respect to different secondary amines under the developed reaction conditions. As shown in Scheme 4, a range of tertiary amides were obtained in good yields with 1,2,3,4-tetrahydroisoquinoline. The reactions of aldehydes with cyclic secondary amines, such as morpholine, proceeded smoothly to generate the desired amides **5n** and **5o** in high yields, but acyclic amines, such as diethylamine, displayed lower conversion; product **5p** was obtained in a relatively low yield. Finally, the acyclic amine *N*-methylbenzylamine can also be used as a coupling partner and the corresponding amides (**5q** and **5r**) were isolated in 60 and 75% yield, respectively, demonstrating the versatility of this reaction.

To demonstrate the practicality and synthetic value of the protocol, the model reaction was scaled up to 10 mmol under standard reaction conditions and desired product **3m** was obtained in 90% yield (Scheme 5).

Table 2 summarizes different photocatalytic systems for the photocatalytic amidation of 4-nitrobenzaldehyde with pyrrolidine in the presence of various photocatalysts (including phenazinium salt, rose bengal, BODIPY, quinolinium compounds, CAT, Ag/g-C₃N₄, and AQN). As observed from the results in Table 2, the present photocatalytic system is equally or more efficient than those previously reported for this reaction with respect to the reaction time and yield. In addition, the



Scheme 4. Substrate scope of aryl aldehydes and secondary amines. Standard reaction conditions were used and reported yields are those of products isolated.



Scheme 5. Large-scale synthesis.

use of precious-metal catalysts or the employment of nonrecyclable catalysts can be avoided in this catalytic system.

Recyclability of the catalyst

From an economic and environmental point of view, the high stability and recyclability of a catalyst are key factors, especially in industrial and well-designed, green synthetic pathways. For this purpose, the stability and reusability of $\text{Fe}_3\text{O}_4/\text{PDA}/\text{CdS}$ were investigated by using model reactions. After the reaction was completed, the catalyst was separated from the reaction mixture by applying an external magnet, washing it with ethanol, and drying the catalyst at 80°C under vacuum. The catalyst could be reused in the next run without further purification. As shown in Figure 7, the recycled catalyst was reused at least five times consecutively, with only a slight loss of catalytic efficiency. The slight decrease in catalytic activity should be due to the normal loss of catalyst during the workup procedure.

After the fifth cycle, the reused catalyst was analyzed by means of FTIR and SEM. The results showed that the catalyst fully maintained its chemical integrity by comparing the FTIR spectrum with that of the fresh catalyst (Figure S2 in the Supporting Information). SEM images of fresh and recovered catalysts indicated that slight morphological changes occurred (Figure S3 in the Supporting Information). Furthermore, to determine if any metal leaching had occurred, the amount of Cd and Fe was determined by ICP analysis. According to this test, the Cd and Fe contents after the fifth cycle were 0.50 and 0.48 ppm, respectively, in CH_3CN (2 mL). This may be due to the excellent affinity of PDA for CdS, which prevents it from leaching. This result indicated that the synthesized $\text{Fe}_3\text{O}_4/\text{PDA}/\text{CdS}$ catalyst had excellent stability and durability under these reaction conditions and could be used multiple times in catalytic conversion.

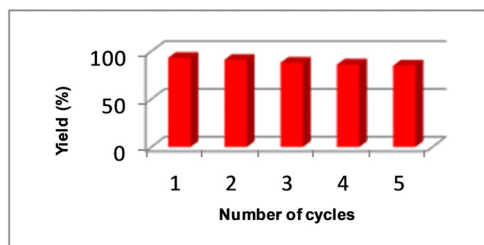


Figure 7. Reusability of the catalyst.

Table 2. A comparison of the efficiency of $\text{Fe}_3\text{O}_4/\text{PDA}/\text{CdS}$ with other reported approaches for the photocatalytic amidation of 4-nitrobenzaldehyde with pyrrolidine.

Entry	Photocatalyst ([mol%])	Reaction conditions ^[a]	Yield [%]	Ref.
1	phenazinium salt (1–2)	air, 24 W lamp, THF, RT, 20 h	75	[32]
2	rose bengal (5)	air, Na_2CO_3 , 25°C , 15 W lamp, CH_3CN , 48 h	40	[33]
3	BODIPY (2)	air, 3 W blue LEDs, dioxane, BHT, RT, 12 h	75	[34]
4	quinolinizinium (5)	air, Na_2CO_3 , blue LEDs, RT, CH_3CN , 48 h	86	[35]
5	CAT (1)	air, visible light, RT, $\text{DMSO}/\text{H}_2\text{O}$ (1:1), 12 h	82	[36]
6	$\text{Ag}/\text{g}-\text{C}_3\text{N}_4$ (5)	air, 25 W CFL, THF, RT, 30 h	78	[37]
7	AQN (1)	O_2 , 21 W CFL, THF, RT, 20 h	49	[38]
8	$\text{Fe}_3\text{O}_4/\text{PDA}/\text{CdS}$ (6.4)	air, 10 W blue LEDs, RT, CH_3CN , 16 h	93	this work

[a] BHT = 2,6-di-*tert*-butyl-4-methylphenol, CFL = compact fluorescent light.

Mechanism study

To elucidate the possible reaction mechanism, some control experiments were performed (Scheme 6). From the optimization research, we know that this reaction does not work in the dark, which implies the importance of visible light. Also, we did not obtain any product if the model reaction was performed under an inert atmosphere, indicating the role of oxygen in the air in this reaction. In addition, the model reaction was carried out in the presence of TEMPO or BHT, which significantly reduced the yield of **3m**, indicating the existence of free-radical pathways. Meanwhile, we found that the TEMPO- and BHT-trapped products **A** and **B** could be identified by mass spectrometry. In addition, only 10% yield of **3m** could be achieved if the superoxide radical ($\text{O}_2^{\cdot-}$) scavenger DMPO was added to the reaction mixture.

Based on these investigations and previous related reports,^[34,38] a plausible mechanism for the photoinduced amidation reaction is depicted in Scheme 6. Initially, the free amine undergoes nucleophilic attack to the aldehyde to give the intermediate (4-nitrophenyl)(pyrrolidin-1-yl)methanol (**I**). Upon irradiation with a blue LED, charge carriers of h^+ and e^- are generated on the surface of the photocatalyst.^[79] PDA can be used as a photosensitizer for the activation of CdS under visible light.^[74] In addition, the PDA shell has the ability to undergo light-induced hole formation under light irradiation, which can extend the recombination rate of photoinduced electrons and holes.^[75] The photoexcited electrons in the CB can reduce surface-absorbed O_2 to form a superoxide radical, which further extracts one proton from intermediate **I**, producing anionic (4-nitrophenyl)(pyrrolidin-1-yl)methanol (intermediate **II**) and a hydroperoxyl

radical (OOH^{\cdot}) species. Intermediate **II** is further oxidized by photogenerated h^+ to give radical intermediate **III**, which is subsequently oxidized by OOH^{\cdot} to give desirable final product **3m**. In the proposed catalytic process, byproduct H_2O_2 can be detected by adding excess saturated NaI to the post-photocatalytic reaction solution, in which triiodide (I_3^-) species with a characteristic UV/Vis absorption band at 350 nm will be formed through the reaction of H_2O_2 with an excess amount of I^- .^[80]

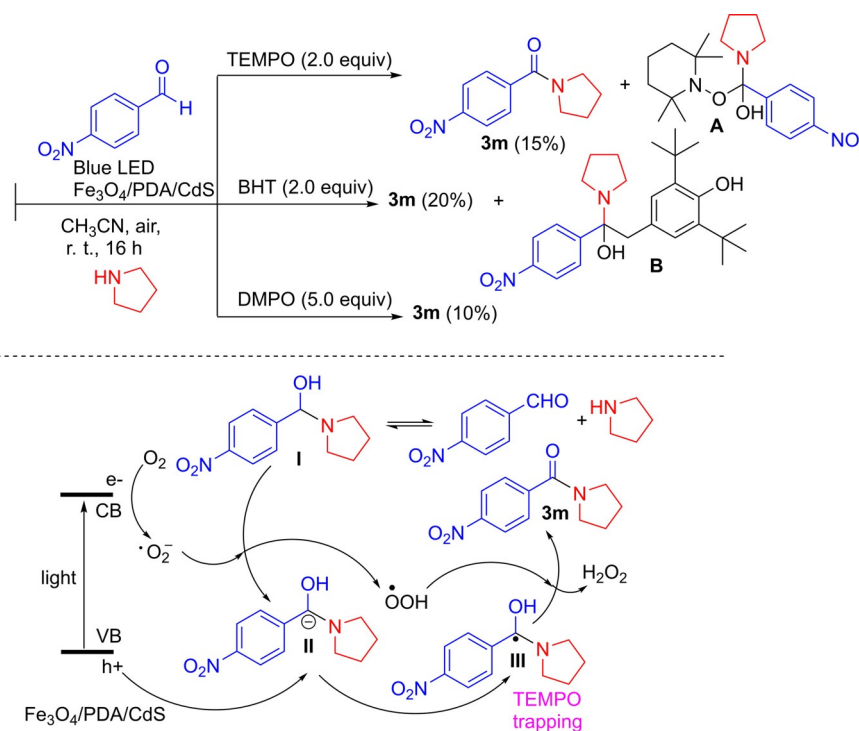
Conclusion

We have demonstrated that magnetic CdS quantum dots can be used as an efficient visible-light-active photocatalyst for the oxidative amidation of aromatic aldehydes with amines by using air as a clean oxidant. This method avoids the use of expensive catalysts, strong bases, and large amounts of other additives. Furthermore, the magnetic catalyst is very stable under the reaction conditions and can be easily recovered and reused for five cycles without any decrease in the catalytic activity. This new approach meets the requirements of green chemistry and opens up a new avenue for the development of more sustainable organic reactions for constructing synthetically important molecules under visible-light irradiation.

Experimental Section

General

All chemicals and reagents were obtained from commercial suppliers and used as received without further purification. Melting points were determined on an X-5 instrument and were uncorrect-



Scheme 6. Control experiments and proposed plausible mechanism for light-promoted amidation. TEMPO = 2,2,6,6-tetramethylpiperidinyloxy, DMPO = 5,5-dimethyl-1-pyrroline *N*-oxide, VB = valence band, CB = conduction band.

ed. IR spectra were recorded in the range of 400–4000 cm^{-1} on a Bruker Tensor 27 FTIR spectroscope as KBr disks. Power XRD data were obtained on a Bruker D8 Advance X-ray diffractometer, $\text{Cu}_{\text{K}\alpha}$ was used as the X-ray source, and the scanning rate was 0.05°s^{-1} between 20 and 80° . TEM was performed on a Hitachi H-7650 instrument running at 80 kV. A scanning electron microscope equipped with an INCA 350 energy-dispersive spectrometer accessory was used on a Hitachi S-4800 SEM instrument to study the surface morphology and elemental composition of the catalyst. ^1H and ^{13}C NMR spectroscopy data were acquired on a Zhongke Niujin AS 400 spectrometer (400 MHz for ^1H NMR spectroscopy and 100 MHz for ^{13}C NMR spectroscopy) by using tetramethylsilane (TMS) as an internal standard. Mass spectra were recorded on a 3200 Qtrap instrument with an ESI source. The N_2 adsorption–desorption isotherms were measured at 77 K by using an automatic surface area and pore analyzer. ICP-AES analyses were performed with an X Series 2 spectrometer. Irradiation experiments were carried out on a WP-VLH-1020 photoreactor (Xi'an WATTECS Experimental Equipment Co.)

Preparation of Fe_3O_4

Fe_3O_4 NPs were prepared as reported by our group with modifications. $\text{FeCl}_3\cdot 6\text{H}_2\text{O}$ (20 mmol, 5.40 g) and $\text{FeCl}_2\cdot 4\text{H}_2\text{O}$ (10 mmol, 1.98 g) were dissolved in distilled water (100 mL) in a three-necked flask under sonication for 15 min. Ammonia solution (25% v/v) was added slowly to adjust the pH of the solution to 10. The reaction mixture was then continually stirred at 60°C for 1 h. The magnetic Fe_3O_4 NPs were separated by using an external magnet, washed with water followed by ethanol, and dried under vacuum at 80°C for 24 h.

Surface modification of Fe_3O_4

Fe_3O_4 (2 g) was dispersed in water (25 mL) under sonication for 30 min. Dopamine hydrochloride (2 g) dissolved in water (5 mL) was added to the above solution and again sonicated for 2 h. Amine-functionalized Fe_3O_4 was precipitated with acetone, isolated by using an external magnet, and dried under vacuum at 60°C for 2 h.

Synthesis of Fe_3O_4 /PDA/CdS nanocomposites

Amine-functionalized Fe_3O_4 (2 g) was added to an aqueous solution (25 mL) containing $\text{Cd}(\text{NO}_3)_2\cdot 4\text{H}_2\text{O}$ (8 mmol) and thiourea (8 mmol). Then the reaction mixture was exposed to ultrasound for 30 min, followed by heating at 80°C for 15 min. An aqueous solution of sodium hydroxide (1 molL^{-1}) was added dropwise to bring the pH of this mixture to 8.0, and the resulting slurry was stirred for 30 min at room temperature. The resulting brownish solids were separated magnetically, washed several times with water and ethanol, and dried under vacuum at 70°C for 5 h.

General procedure for the oxidative amidation of aromatic aldehydes with amines

To a 15 mL quartz tube equipped with a magnetic stirrer bar, aldehyde (1 mmol), amine (1 mmol), and Fe_3O_4 /PDA/CdS (20 mg, 6.4 mol% Cd) were added successively in CH_3CN (3 mL). The reaction tube was exposed to blue LED (450–460 nm, 10 W) irradiation at a distance of approximately 3 mm from the bottom of the tube at room temperature under air with stirring for an appropriate time. Upon completion of the reaction (monitored by TLC), the reaction mixture turned clear and catalyst was deposited on the

magnetic bar, which was easily removed from the reaction mixture by using an external magnet. The recovered catalyst was washed with EtOH, dried under the vacuum, and reused. The organic layer was evaporated and the crude product was purified by column chromatography on silica gel to obtain the desired, pure compound.

Acknowledgements

Financial support from the Nature Science Foundation of Hebei Province (B2020205026), the National Natural Science Foundation of China (21272053), the Science Technology Research Foundation of Hebei Normal University (L2018Z06), and the Graduate Innovation Funding Program of Hebei Normal University (CXZZSS2020040) is gratefully acknowledged.

Conflict of interest

The authors declare no conflict of interest.

Keywords: amidation · heterogeneous catalysis · magnetic properties · photochemistry · quantum dots

- [1] L. Vaccaro, *Eur. J. Org. Chem.* **2020**, 4273–4283.
- [2] F. Strieth-Kalthoff, M. J. James, M. Teders, L. Pitzer, F. Glorius, *Chem. Soc. Rev.* **2018**, 47, 7190–7202.
- [3] a) M. Zhang, W. Sun, H. Lv, Z.-H. Zhang, *Curr. Opin. Green. Sustain. Chem.* **2021**, 27, 100390; b) M. Zhang, Z. Li, X. Xin, J. Zhang, Y. Feng, H. Lv, *ACS Catal.* **2020**, 10, 14793–14800.
- [4] C. L. Bian, A. K. Singh, L. B. Niu, H. Yi, A. W. Lei, *Asian J. Org. Chem.* **2017**, 6, 386–396.
- [5] Q. Q. Zhou, Y. Q. Zou, L. Q. Lu, W. J. Xiao, *Angew. Chem. Int. Ed.* **2019**, 58, 1586–1604; *Angew. Chem.* **2019**, 131, 1600–1619.
- [6] a) M. Parasram, V. Gevorgyan, *Chem. Soc. Rev.* **2017**, 46, 6227–6240; b) M. Zhu, X. Han, W. J. Fu, Z. Q. Wang, B. M. Hao, X. Q. Hao, M. P. Song, C. Xu, *J. Org. Chem.* **2016**, 81, 7282–7287; c) M. Zhu, R. X. Li, Q. Q. You, W. J. Fu, W. S. Guo, *Asian J. Org. Chem.* **2019**, 8, 2002–2005.
- [7] S. Fukuzumi, K. Ohkubo, *Org. Biomol. Chem.* **2014**, 12, 6059–6071.
- [8] M. N. Chen, J. Q. Di, J. M. Li, L. P. Mo, Z. H. Zhang, *Tetrahedron* **2020**, 76, 131059.
- [9] A. Vijeta, E. Reisner, *Chem. Commun.* **2019**, 55, 14007–14010.
- [10] J. J. Wang, L. S. Xue, M. Hong, B. Q. Ni, T. F. Niu, *Green Chem.* **2020**, 22, 411–416.
- [11] M. Tian, S. Y. Liu, X. B. Bu, J. P. Yu, X. B. Yang, *Chem. Eur. J.* **2020**, 26, 369–373.
- [12] Y. X. Lin, J. Guo, J. San Martin, C. Han, R. Martinez, Y. Yan, *Chem. Eur. J.* **2020**, 26, 13118–13136.
- [13] Y. R. Girish, R. Biswas, M. De, *Chem. Eur. J.* **2018**, 24, 13871–13878.
- [14] R. M. de Figueiredo, J. S. Suppo, J. M. Campagne, *Chem. Rev.* **2016**, 116, 12029–12122.
- [15] D. W. Zhang, X. Zhao, J. L. Hou, Z. T. Li, *Chem. Rev.* **2012**, 112, 5271–5316.
- [16] C. L. Allen, J. M. J. Williams, *Chem. Soc. Rev.* **2011**, 40, 3405–3415.
- [17] E. Massolo, M. Pirola, M. Benaglia, *Eur. J. Org. Chem.* **2020**, 4641–4651.
- [18] H. F. Motiwala, M. Charaschanya, V. W. Day, J. Aube, *J. Org. Chem.* **2016**, 81, 1593–1609.
- [19] J. Zhang, Y. Y. Liu, W. C. Feng, Y. M. Wu, *Chin. J. Org. Chem.* **2019**, 39, 961–997.
- [20] C. Bednarek, I. Wehl, N. Jung, U. Schepers, S. Brase, *Chem. Rev.* **2020**, 120, 4301–4354.
- [21] S. Kang, M. T. La, H. K. Kim, *Tetrahedron Lett.* **2018**, 59, 3541–3546.
- [22] K. Kim, A. M. P. Moeljadi, H. Hirao, S. H. Hong, *Adv. Synth. Catal.* **2017**, 359, 3292–3298.

- [23] S. R. Mudshinge, C. S. Potnis, B. Xu, G. B. Hammond, *Green Chem.* **2020**, *22*, 4161–4164.
- [24] S. De Sarkar, A. Studer, *Org. Lett.* **2010**, *12*, 1992–1995.
- [25] R. Cadoni, A. Porcheddu, G. Giacomelli, L. De Luca, *Org. Lett.* **2012**, *14*, 5014–5017.
- [26] J. F. Wang, J. M. Li, F. Xu, Q. Shen, *Adv. Synth. Catal.* **2009**, *351*, 1363–1370.
- [27] S. C. Ghosh, J. S. Y. Ngiam, A. M. Seayad, D. T. Tuan, C. L. L. Chai, A. Q. Chen, *J. Org. Chem.* **2012**, *77*, 8007–8015.
- [28] W. J. Yoo, C. J. Li, *J. Am. Chem. Soc.* **2006**, *128*, 13064–13065.
- [29] Y. M. Li, F. Jia, Z. P. Li, *Chem. Eur. J.* **2013**, *19*, 82–86.
- [30] J. W. W. Chang, P. W. H. Chan, *Angew. Chem. Int. Ed.* **2008**, *47*, 1138–1140; *Angew. Chem.* **2008**, *120*, 1154–1156.
- [31] Y. Cao, W. D. Sun, G. Luo, Y. Yu, Y. H. Zhou, Y. N. Zhao, J. M. Yang, Y. Luo, *Org. Lett.* **2020**, *22*, 705–708.
- [32] D. Leow, *Org. Lett.* **2014**, *16*, 5812–5815.
- [33] F. K. C. Leung, J. F. Cui, T. W. Hui, K. K. Y. Kung, M. K. Wong, *Asian J. Org. Chem.* **2015**, *4*, 533–536.
- [34] X. F. Wang, S. S. Yu, C. Wang, D. Xue, J. L. Xiao, *Org. Biomol. Chem.* **2016**, *14*, 7028–7037.
- [35] J. R. Deng, W. C. Chan, N. C. H. Lai, B. Yang, C. S. Tsang, B. C. B. Ko, S. L. F. Chan, M. K. Wong, *Chem. Sci.* **2017**, *8*, 7537–7544.
- [36] H. Deol, M. Kumar, V. Bhalla, *RSC Adv.* **2018**, *8*, 31237–31245.
- [37] L. L. Wang, M. Yu, C. L. Wu, N. Deng, C. Wang, X. Q. Yao, *Adv. Synth. Catal.* **2016**, *358*, 2631–2641.
- [38] H. Inagawa, S. Uchida, E. Yamaguchi, A. Itoh, *Asian J. Org. Chem.* **2019**, *8*, 1411–1414.
- [39] a) D. Friedmann, A. Hakki, H. Kim, W. Choic, D. Bahnemann, *Green Chem.* **2016**, *18*, 5391–5411; b) Y. H. Li, F. Zhang, Y. Chen, J. Y. Li, Y. J. Xu, *Green Chem.* **2020**, *22*, 163–169; c) B. Weng, M.-Y. Qi, C. Han, Z.-R. Tang, Y.-J. Xu, *ACS Catal.* **2019**, *9*, 4642–4687.
- [40] a) G. B. Wang, S. Li, C. X. Yan, F. C. Zhu, Q. Q. Lin, K. H. Xie, Y. Geng, Y. B. Dong, *J. Mater. Chem. A* **2020**, *8*, 6957–6983; b) C. Han, S. H. Li, Z. R. Tang, Y. J. Xu, *Chem. Sci.* **2018**, *9*, 8914–8922; c) C. Han, Z. R. Tang, J. X. Liu, S. Y. Jin, Y. J. Xu, *Chem. Sci.* **2019**, *10*, 3514–3522; d) J. Y. Li, Y. H. Li, F. Zhang, Z. R. Tang, Y. J. Xu, *Appl. Catal. B* **2020**, *269*, 118783; e) Y. H. Li, M. Y. Yi, J. Y. Li, Z. R. Tang, Y. J. Xu, *Appl. Catal. B* **2019**, *257*, 117934.
- [41] X. J. Lang, W. H. Ma, Y. B. Zhao, C. C. Chen, H. W. Ji, J. C. Zhao, *Chem. Eur. J.* **2012**, *18*, 2624–2631.
- [42] a) Y. L. Yang, D. N. Zhang, Q. J. Xiang, *Nanoscale* **2019**, *11*, 18797–18805; b) N. Zhang, S. H. Li, X. Z. Fu, Y. J. Xu, *Pure Appl. Chem.* **2018**, *90*, 1379–1392.
- [43] M. Q. Yang, Y. J. Xu, *Phys. Chem. Chem. Phys.* **2013**, *15*, 19102–19118.
- [44] a) L. Cheng, Q. J. Xiang, Y. L. Liao, H. W. Zhang, *Energy Environ. Sci.* **2018**, *11*, 1362–1391; b) Z. R. Tang, B. Han, C. Han, Y. J. Xu, *J. Mater. Chem. A* **2017**, *5*, 2387–2410; c) R. C. Shen, D. D. Ren, Y. N. Ding, Y. T. Guan, Y. H. Ng, P. Zhang, X. Li, *Sci. China Mater.* **2020**, *63*, 2153–2188.
- [45] J. Y. Li, Y. H. Li, M. Y. Qi, Q. Lin, Z. R. Tang, Y. J. Xu, *ACS Catal.* **2020**, *10*, 6262–6280.
- [46] H. Y. Wang, R. Hu, Y. J. Lei, Z. Y. Jia, G. L. Hu, C. B. Li, Q. Gu, *Catal. Sci. Technol.* **2020**, *10*, 2821–2829.
- [47] B. T. Sun, Z. Q. Liang, Y. Y. Qian, X. S. Xu, Y. Han, J. Tian, *ACS Appl. Mater. Interfaces* **2020**, *12*, 7257–7269.
- [48] K. Singha, A. Mondal, S. C. Ghosh, A. B. Panda, *Chem. Asian J.* **2018**, *13*, 255–260.
- [49] C. Huang, X. B. Li, C. H. Tung, L. Z. Wu, *Chem. Eur. J.* **2018**, *24*, 11530–11534.
- [50] J. L. Hu, T. J. Pu, Z. W. Xu, W. Y. Xu, Y. S. Feng, *Adv. Synth. Catal.* **2019**, *361*, 708–713.
- [51] S. Firoozi, M. Hosseini-Sarvari, *Eur. J. Org. Chem.* **2020**, 3834–3843.
- [52] S. Firoozi, M. Hosseini-Sarvari, M. Koohgard, *Green Chem.* **2018**, *20*, 5540–5549.
- [53] X. F. Ning, S. G. Meng, X. L. Fu, X. J. Ye, S. F. Chen, *Green Chem.* **2016**, *18*, 3628–3639.
- [54] Z. W. Xi, L. Yang, D. Y. Wang, C. D. Pu, Y. M. Shen, C. D. Wu, X. G. Peng, *J. Org. Chem.* **2018**, *83*, 11886–11895.
- [55] S. Das, S. Samanta, S. K. Maji, P. K. Samanta, A. K. Dutta, D. N. Srivastava, B. Adhikary, P. Biswas, *Tetrahedron Lett.* **2013**, *54*, 1090–1096.
- [56] a) J. L. DiMeglio, A. G. Breuhaus-Alvarez, S. Q. Li, B. M. Bartlett, *ACS Catal.* **2019**, *9*, 5732–5741; b) M.-Y. Qi, Y.-H. Li, M. Anpo, Z.-R. Tang, Y.-J. Xu, *ACS Catal.* **2020**, *10*, 14327–14335.
- [57] X. F. Ning, W. L. Zhen, Y. Q. Wu, G. X. Lu, *Appl. Catal. B* **2018**, *226*, 373–383.
- [58] L. Cheng, D. Zhang, Y. Liao, H. Zhang, Q. Xiang, *Solar Rrl* **2019**, *3*, 1900062.
- [59] D. D. Ren, Z. Z. Liang, Y. H. Ng, P. Zhang, Q. J. Xiang, X. Li, *Chem. Eng. J.* **2020**, *390*, 124496.
- [60] Q. J. Xiang, F. Y. Cheng, D. Lang, *ChemSusChem* **2016**, *9*, 996–1002.
- [61] Y. Lin, Q. Zhang, Y. H. Li, Y. P. Liu, K. J. Xu, J. N. Huang, X. S. Zhou, F. Peng, *ACS Sustainable Chem. Eng.* **2020**, *8*, 4537–4546.
- [62] Y. Y. Dong, Y. L. Su, Y. F. Hu, H. X. Li, W. Xie, *Small* **2020**, *16*, 2001529.
- [63] L. L. Zhang, H. W. Zhang, B. Wang, X. Y. Huang, Y. Ye, R. Lei, W. H. Feng, P. Liu, *Appl. Catal. B* **2019**, *244*, 529–535.
- [64] a) R. K. Sharma, S. Dutta, S. Sharma, R. Zboril, R. S. Varma, M. B. Gawande, *Green Chem.* **2016**, *18*, 3184–3209; b) M. N. Chen, L. P. Mo, Z. S. Cui, Z. H. Zhang, *Curr. Opin. Green. Sustain. Chem.* **2019**, *15*, 27–37; c) G. Gao, J. Q. Di, H. Y. Zhang, L. P. Mo, Z. H. Zhang, *J. Catal.* **2020**, *387*, 39–46; d) M. B. Gawande, Y. Monga, R. Zboril, R. K. Sharma, *Coord. Chem. Rev.* **2015**, *288*, 118–143; e) M. Zhang, Y. H. Liu, Z. R. Shang, H. C. Hu, Z. H. Zhang, *Catal. Commun.* **2017**, *88*, 39–44.
- [65] P. Eskandari, F. Kazemi, *J. Photochem. Photobiol. A* **2018**, *364*, 233–239.
- [66] A. Samadi-Maybodi, M. R. Shariati, A. H. Colagar, *ChemPlusChem* **2018**, *83*, 769–779.
- [67] Z. Y. Lu, X. X. Zhao, Z. Zhu, Y. S. Yan, W. D. Shi, H. J. Dong, Z. F. Ma, N. L. Gao, Y. S. Wang, H. Huang, *Chem. Eur. J.* **2015**, *21*, 18528–18533.
- [68] W. Shi, D. Du, B. Shen, C. F. Cui, L. J. Lu, L. Z. Wang, J. L. Zhang, *ACS Appl. Mater. Interfaces* **2016**, *8*, 20831–20838.
- [69] W. Shi, D. L. Lu, L. Z. Wang, F. Teng, J. L. Zhang, *RSC Adv.* **2015**, *5*, 106038–106043.
- [70] J. H. Yang, J. Wang, X. Y. Li, D. D. Wang, H. Song, *Catal. Sci. Technol.* **2016**, *6*, 4525–4534.
- [71] R. Shen, L. Zhang, X. Chen, M. Jaroniec, N. Li, X. Li, *Appl. Catal. B* **2020**, *266*, 118619.
- [72] a) H. A. Lee, Y. F. Ma, F. Zhou, S. Hong, H. Lee, *Acc. Chem. Res.* **2019**, *52*, 704–713; b) J. H. Ryu, P. B. Messersmith, H. Lee, *ACS Appl. Mater. Interfaces* **2018**, *10*, 7523–7540.
- [73] A. M. Xie, K. Zhang, F. Wu, N. N. Wang, Y. Wang, M. Y. Wang, *Catal. Sci. Technol.* **2016**, *6*, 1764–1771.
- [74] W. X. Mao, X. J. Lin, W. Zhang, Z. X. Chi, R. W. Lyu, A. M. Cao, L. J. Wan, *Chem. Commun.* **2016**, *52*, 7122–7125.
- [75] J. J. Feng, P. P. Zhang, A. J. Wang, Q. C. Liao, J. L. Xi, J. R. Chen, *New J. Chem.* **2012**, *36*, 148–154.
- [76] a) H. Veisi, T. Tamoradi, A. Rashtiani, S. Hemmati, B. Karmakar, *J. Ind. Eng. Chem.* **2020**, *90*, 379–388; b) H. Veisi, P. Sarachegol, S. Hemmati, *Polyhedron* **2018**, *156*, 64–71.
- [77] a) Y. Han, M. Zhang, Y. Q. Zhang, Z. H. Zhang, *Green Chem.* **2018**, *20*, 4891–4900; b) H. J. Wang, M. Zhang, W. J. Li, Y. Ni, J. Lin, Z. H. Zhang, *Adv. Synth. Catal.* **2019**, *361*, 5018–5024; c) J. Q. Di, M. Zhang, Y. X. Chen, J. X. Wang, S. S. Geng, J. Q. Tang, Z. H. Zhang, *Green Chem.* **2021**, *23*, 1041–1049.
- [78] a) M. Zhang, Q. Y. Fu, G. Gao, H. Y. He, Y. Zhang, Y. S. Wu, Z. H. Zhang, *ACS Sustainable Chem. Eng.* **2017**, *5*, 6175–6182; b) M. Zhang, M. N. Chen, Z. H. Zhang, *Adv. Synth. Catal.* **2019**, *361*, 5182–5190.
- [79] Z. G. Chai, T. T. Zeng, Q. Li, L. Q. Lu, W. J. Xiao, D. S. Xu, *J. Am. Chem. Soc.* **2016**, *138*, 10128–10131.
- [80] W. Huang, B. C. Ma, H. Lu, R. Li, L. Wang, K. Landfester, K. A. I. Zhang, *ACS Catal.* **2017**, *7*, 5438–5442.

Manuscript received: November 28, 2020
Revised manuscript received: January 1, 2021
Accepted manuscript online: January 5, 2021
Version of record online: February 25, 2021